Solution Structure of a DNA Decamer Containing the Antiviral Drug Ganciclovir: Combined Use of NMR, Restrained Molecular Dynamics, and Full Relaxation Matrix Refinement‡

Matthew Foti,[§,||] Stephen Marshalko,[⊥] Eric Schurter,[§] Surat Kumar,[§] G. Peter Beardsley,[⊥] and Barry I. Schweitzer*[,§,#]

Walt Disney Memorial Cancer Institute at Florida Hospital, 12722 Research Parkway, Orlando, Florida 32826, Department of Chemistry, University of South Florida, Tampa, Florida 33620-8800, Department of Chemistry, University of Central Florida, Orlando, Florida 32826, and Department of Pediatrics, Yale University School of Medicine, New Haven, Connecticut 06510

Received October 17, 1996; Revised Manuscript Received February 19, 1997[⊗]

ABSTRACT: The nucleoside analog 9-[(1,3-dihydroxy-2-propoxy)methyl]guanine (ganciclovir, DHPG) is an antiviral drug that is used in the treatment of a variety of herpes viruses in immunocompromised patients and in a gene therapy protocol that has shown promising activity for the treatment of cancer. To probe the structural effects of ganciclovir when incorporated into DNA, we determined and compared the solution structure of a modified ganciclovir-containing decamer duplex $[d(CTG)(ganciclovir)d(ATCCAG)]_2$ and a control duplex $d[(CTGGATCCAG)]_2$ using nuclear magnetic resonance techniques. ^1H and ^{31}P resonances in both duplexes were assigned using a combination of 2-D ^1H and ^{31}P NMR experiments. Proton−proton distances determined from NOESY data and dihedral angles determined from DQF-COSY data were used in restrained molecular dynamics simulations starting from canonical A- and B-form DNA models. Both the control and ganciclovir sets of simulations converged to B-type structures. These structures were subjected to full relaxation matrix refinement to produce final structures that were in excellent agreement with the observed NOE intensities. Examination of the final ganciclovir-containing structures reveals that the base of the ganciclovir residue is hydrogen bonded to its complementary dC and is stacked in the helix; in fact, the base of ganciclovir exhibits increased stacking with the 5′ base relative to the control. Interestingly, some of the most significant distortions in the structures occur 3′ to the lesion site, including a noticeable kink in the sugar−phosphate backbone at this position. Further examination reveals that the backbone conformation, sugar pucker, and glycosidic torsion angle of the residue 3′ to the lesion site all indicate an A-type conformation at this position. A possible correlation of these structural findings with results obtained from earlier biochemical studies will be discussed.

The compound 9-[(1,3-dihydroxy-2-propoxy)methyl]guanine (ganciclovir, Figure 1) is an effective antiviral agent used to treat HSV[1] and CMV infections. It is used primarily in the clinic to treat life-threatening CMV infections in AIDS patients and in other immunocompromised patients such as those undergoing chemotherapy or bone marrow transplants (Erice et al., 1987; Zaia, 1993; Buckner & Pomeroy, 1993; Nevins & Dunn, 1992; Faulds & Heel, 1990; Emmanuel, 1990). Recently, the use of ganciclovir in combination with a gene therapy protocol involving the HSV thymidine kinase gene has shown promise in the treatment of a variety of human malignancies, including brain (Culver et al., 1992, 1994; Smythe et al., 1994; Chen et al., 1994), lung (Hasegawa et al., 1995), liver (Ido et al., 1995), stomach (Yoshida et al., 1995), breast (Manome et al., 1994), and pancreas (DiMaio et al., 1994). Ganciclovir is selective toward virally infected cells since it is converted to the monophosphate form only by viral encoded kinases. Cellular kinases then convert the monophosphate to the diphosphate and the active triphosphate form. Possible modes of action for the triphosphate form include competitive inhibition of DNA polymerases and/or misincorporation into newly synthesized DNA where it interferes with further DNA replication.

Ganciclovir is structurally similar to deoxyguanosine (Figure 1) but lacks the 2′ carbon atom of deoxyguanosine and is therefore an acyclic nucleoside. It still retains the equivalent of 3′- and 5′-hydroxyls so it can be incorporated into DNA at both internal positions and terminal positions. Removing the 2′ carbon atom in ganciclovir creates a prochiral center at what is normally the 4′ carbon atom (Figure 1). This stereochemistry is relevant during the biochemical conversion to the mono-, di-, and triphosphate forms; HSV thymidine kinase is stereospecific for the *pro-S* hydroxyl group (Karkas et al., 1987), and only the (*S*)-monophosphate is converted by GMP kinase to the diphosphate (Tolman, 1989). The detailed study of DNA oligomers containing ganciclovir has not been possible due to stereochemical synthetic barriers. Recently, we have designed a chiral chemical synthesis of the phosphoramidite of ganciclovir (Marshalko et al., 1995). The key chemical step in our synthetic scheme employs porcine pancreatic lipase to catalyze a stereospecific acetyl transfer reaction to the *pro-S*

‡ The coordinates have been deposited with the Brookhaven Protein Data Bank under the name 1ac9.

* To whom correspondence should be addressed.
§ Walt Disney Memorial Cancer Institute at Florida Hospital.
|| University of South Florida.
⊥ Yale University School of Medicine.
University of Central Florida.

⊗ Abstract published in *Advance ACS Abstracts,* April 1, 1997.

[1] Abbreviations: CMV, cytomegalovirus; HSV, herpes simplex virus; NMR, nuclear magnetic resonance; HPLC, high-performance liquid chromatography; NOESY, nuclear Overhauser effect spectroscopy; DMT, dimethoxytrityl; DQF-COSY, double-quantum-filtered correlated spectroscopy; heteroTOCSY, heteronuclear total correlated spectroscopy; Ini-A, canonical A-DNA; Ini-B, canonical B-DNA; rMD, restrained molecular dynamics; RR, relaxation matrix refined; RMSD, root mean square deviation; ganciclovir, 9-[(1,3-dihydroxy-2-propoxy)-methyl]guanine.

S0006-2960(96)02604-9 CCC: $14.00 © 1997 American Chemical Society

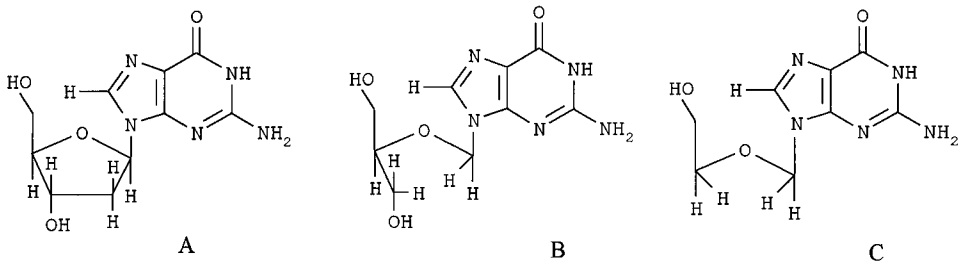

FIGURE 1: Chemical structure of ganciclovir: (A) deoxyguanosine; (B) ganciclovir; (C) acyclovir.

Control Duplex:

5'-C_1 $T_2G_3G_4A_5T_6C_7C_8A_9G_{10}$-3'
3'-$G_{10}A_9C_8C_7T_6A_5G_4G_3T_2C_1$-5'

Ganciclovir Duplex:

5'-C_1 $T_2G_3\underline{D}_4A_5T_6C_7C_8A_9G_{10}$-3'
3'-$G_{10}A_9C_8C_7T_6A_5\underline{D}_4G_3T_2C_1$-5'

FIGURE 2: Sequence composition of the control duplex and the ganciclovir duplex. D denotes ganciclovir.

hydroxyl group of ganciclovir, resulting in a single enantiomer, as demonstrated by NMR chiral shift investigations. The absolute stereochemistry was determined by comparison of the rates of utilization by GMP kinase of our chemically synthesized ganciclovir monophosphate with that produced enzymatically by phosphorylation with HSV thymidine kinase. We have used this phosphoramidite and automated chemical synthesis to make DNA containing only the biologically relevant isomer of ganciclovir (Marshalko et al., 1995). This development now allows us to determine the molecular mechanism of ganciclovir action by characterizing the thermodynamic, biochemical, and structural consequences of ganciclovir incorporation into DNA.

To initiate our investigations, we synthesized a self-complementary decamer containing a single ganciclovir residue at position 4 and an identical control sequence with dG at this position (Figure 2). UV absorbance versus temperature studies demonstrated a decrease of 13 °C in the melting temperature of the self-complementary duplex containing two ganciclovir sites, as compared to the control duplex (Marshalko et al., 1995). To extend the investigation to include thermodynamic parameters, the concentration dependence of the melting temperature, the van't Hoff relationship, and the Gibbs relationship were used to estimate the entropy, enthalpy, and free energy of duplex formation. The presence of two ganciclovir sites in a single self-complementary duplex was found to reduce the entropy of duplex formation ($\Delta\Delta S$) by 55 cal/(mol deg) but also significantly reduced the enthalpy of duplex formation ($\Delta\Delta H$) by 19.5 kcal/mol. The free energy of duplex formation ($\Delta\Delta G$) was reduced by 3.3. kcal/mol at 25 °C (Marshalko et al., 1995). These results show that incorporation of ganciclovir significantly reduces the stability of the duplex and that this reduction is due both to the entropic effects of the reduced constraints of the acyclic "sugar" and to the enthalpic effects presumably caused by perturbation-(s) of duplex conformation.

In the present study, we continue our biophysical characterization of the ganciclovir lesion using solution-state NMR. We have obtained complete assignments of the proton and phosphorus resonances for the ganciclovir-containing decamer [d(CTG)(ganciclovir)d(ATCCAG)]$_2$. A set of interproton distances derived from NOESY spectra and dihedral angles from DQF-COSY spectra were used as the basis for structural refinement by restrained molecular dynamics and complete relaxation matrix calculations. A similar procedure was used to determine the solution structure of the control decamer [d(CTGGATCCAG)]$_2$. In both cases, convergence to a B-type structure was achieved starting from either canonical A- or B-type DNA. Although the resulting structure of the ganciclovir-containing DNA indicated that the ganciclovir base participates in Watson−Crick hydrogen bonding and is stacked normally in the helix, significant distortions were observed in the sugar−phosphate backbone localized at or near the site of ganciclovir incorporation. The extent to which this structure is in agreement with thermodynamic and biochemical studies on the ganciclovir lesion will be discussed.

MATERIALS AND METHODS

Sample Preparation. The DNA decamer [d(CTG(ganciclovir)ATCCAG)]$_2$ (also referred to herein as the ganciclovir duplex) and the control decamer [d(CTGGATCCAG)]$_2$ (also referred to herein as the control duplex) were synthesized on an Applied Biosystems automated DNA synthesis machine on a 10 μmol scale. The control duplex was synthesized using standard solid-phase phosphoramidite chemistry. The (*S*)-ganciclovir 3′-DMT-5′ phosphoramidite was prepared using the synthetic scheme previously described (Marshalko et al., 1995). Enantiomeric purity was determined using chiral shift adducts along with ^{1}H and ^{31}P NMR. This synthetic scheme results in the synthesis of a 5′-phosphoramidite rather than the 3′-phosphoramidite standardly used in automated DNA synthesis; consequently, reverse (5′) phosphoramidites (Glen Research Corp.) were used in the automated synthesis of DNA containing ganciclovir. The synthesis of DNA using these precursors is analogous to the standard system and employs identical chemistry; synthesis, however, proceeds in a 5′ to 3′ direction.

The trityl-on deprotected DNA was purified using reverse-phase HPLC to remove failure sequences. The purified trityl-on DNA fractions were lyophilized and suspended in 80% acetic acid for 30 min to remove the trityl group. The detritylated DNA was then repurified using the same HPLC protocol. Pure DNA fractions were combined and lyophilized to dryness. Electrospray negative ion mass spectrum analysis demonstrated a 12 atomic mass unit difference between the control and ganciclovir decamers, consistent with the single carbon atom difference between ganciclovir and deoxyguanosine. For measurements in H_2O, the purified (>95%) DNA was dissolved in 0.25 mL of buffer containing 50 mM NaCl, 25 mM sodium phosphate, 0.02% sodium

azide, pH 6.84, and 10% D_2O, and the sample was placed in a Shigemi microtube (Shigemi Inc.). For measurements in D_2O, the DNA was repeatedly lyophilized to dryness, first from the aqueous buffer and then from 99.996% D_2O. Finally, 0.25 mL of 99.996% D_2O was added to give a duplex concentration of 1.5 mM.

NMR Spectroscopy. All NMR experiments were performed on a Varian 600 MHz Unity Plus NMR spectrometer at a regulated temperature of 10 °C. Four NOESY spectra for the control and the ganciclovir DNA samples with mixing times of 80, 120, 160, and 200 ms were each collected within separate 3 day periods, without removing the sample from the spectrometer. The NOESY data were acquired in the phase-sensitive mode of States et al. (1982) with 2048 complex points in t_2 and 512 complex points in t_1, a relaxation delay of 2.5 s (during which time the residual HDO peak was irradiated), and a spectral width of 6250 Hz. The 200 ms NOESY spectra for the control and the ganciclovir DNA in H_2O were acquired with an excitation sculpting pulse sequence for solvent suppression (Callihan et al., 1996). Selective 180° pulses were applied with a SEDUCE profile to suppress the water resonance. Gradient pulses were applied along the *z* axis for 1 ms at 15 and 3 G/cm with 50 μs delays before and after the gradient pulses. These experiments were collected with States−TPPI phase cycling with 2048 complex points in t_2 and 1024 complex points in t_1, a relaxation delay of 2.5 s, and a spectral width of 12 500 Hz. The two-dimensional $^1H-^{31}P$ heteroTOCSY experiment was performed as previously described (Kellogg & Schweitzer, 1993) with a mixing time of 50 ms. The sweep width used was 1000 Hz for ^{31}P (ω_1) and 3600 for ^1H (ω_2) with 96 and 2048 complex points acquired in the t_1 and t_2 dimensions, respectively.

NMR data were processed using FELIX 95.0 (Molecular Simulations, Inc.). NOESY data sets acquired in D_2O or H_2O were processed with a squared-sine bell shifted 90° window function in the direct dimension and a squared-sine bell shifted 90° window function in the indirect dimension. Data in both dimensions were zero-filled to 2048 real points, Fourier transformed, phased to pure absorption, and baseline corrected with a fifth order polynomial. NOE cross-peak volumes were obtained by cross-peak integration using the FELIX software. The DQF-COSY data sets were apodized with unshifted sine bells in both dimensions, followed by zero-filling to 2048 real points in both dimensions prior to Fourier transformation. ^{31}P resonances are referenced to an external sample of trimethyl phosphate. ^1H resonances are referenced to an external sample of sodium 2,2-dimethyl-2-silapentane-5-sulfonate in an identical buffer.

Determination of Interproton Distances. Initial buildup rates were calculated by fitting the cross-peak volumes at 80, 120, 160, and 200 ms mixing times to a linear equation. These rates (R_{ij}) were converted to distances (r_{ij}) using the cytosine H5−H6 distance of 2.45 Å as the reference distance (r_{ref}), the averaged rate calculated from well-resolved H5−H6 cross peaks (R_{ref}), and the relationship $r_{ij} = r_{ref}(R_{ref}/R_{ij})^{1/6}$. Cross-peak volumes obtained from the exchangeable protons in the 200 ms NOESY acquired in H_2O were also referenced to the H5−H6 interproton distance of 2.45 Å. These distances were given upper and lower bounds according to the following guidelines: for $r_{ij} \leq 2.0$ Å, the errors given were −0.2/+0.2 Å; for 2.0 Å $< r_{ij} \leq$ 2.5 Å, they were −0.2/+0.4 Å; for 2.5 Å $< r_{ij} \leq$ 3.3 Å, they were −0.3/+0.5 Å; and for 3.3 Å $< r_{ij} \leq$ 5.0 Å, they were −0.5/+0.7 Å (Nilges et al., 1987). All distances involving exchangeable protons were given upper and lower bounds of 0.7 Å.

Structure Refinement Protocol. (1) Restraints. In addition to the experimentally determined interproton distance constraints and sugar ring dihedral angles used in restrained molecular dynamics, the α, β, γ, ϵ, and ζ backbone torsion angles were restrained to a range covering both right-handed A- and B-DNA as well as satisfying the torsion angle values measured in both fiber diffraction and single crystal structures of all right-handed DNAs (Gronenborn & Clore, 1989; Baleja et al., 1990). Since there is no *a priori* reason for the backbone at the ganciclovir site to fall into the above range, the conservative approach was taken that no restraints were used for any torsion angle involving the ganciclovir residue. Similarly, no backbone restraints were used at the corresponding dG residue in the control duplex in order to avoid bias. Additional restraints used to preserve the right-handed character and to maintain appropriate base pairing were similar to those previously described (Schweitzer et al., 1994).

(2) Restrained Molecular Dynamics. Initial starting structures were generated by constructing the [d(CTGGATCCAG)]$_2$ duplex in canonical A- or B-form and then removing the C2′ carbon of the G4 and G14 residues using the Biopolymer module of InsightII (version 95.0, Molecular Simulations, Inc.). These unminimized structures are designated Ini-A and Ini-B. All subsequent energy minimizations and molecular dynamics calculations were performed on a Silicon Graphics INDY workstation using the program X-PLOR 3.1 (Brunger, 1993). All structures shown in this work were displayed using InsightII 95.0. Nucleic acid parameters and force constants were obtained from the parameter file parallhdg.dna (X-PLOR 3.1). For the electrostatic component of the empirical energy function, the effect of solvent was approximated by a $1/r$ screening function (Brooks et al., 1993). Since the solution structure of the control duplex has been previously determined by Nilges and co-workers (Nilges et al., 1987), it seemed appropriate to use the same protocol of restrained molecular dynamics calculations as these workers. Each initial structure was minimized followed by a restrained molecular dynamics phase. The dynamics protocol consisted of a heating phase from 200 to 300 K over 1 ps followed by a 43 ps dynamics period during which time the force constant for the distance constraints was gradually increased. The coordinate trajectories from the final 23 ps of this dynamics period were averaged and subsequently minimized to yield the final rMD structure. This procedure was repeated three times from each starting canonical A and canonical B structure, using different random number seeds for each subsequent molecular dynamics run generating six final rMD control duplex structures and six rMD ganciclovir duplex structures.

(3) Relaxation Matrix Refinement. In the final stage of structure determination, direct NOE refinements (Yip & Case, 1989) of the six control and six ganciclovir rMD structures generated as described above were carried out using the RELAX option of X-PLOR (Nilges et al., 1991). Details of the dynamic simulated annealing refinement protocol utilized are given in Schweitzer et al. (1994). $R^{1/6}$ factors were calculated as the weighted average of the absolute value of the difference between the one-sixth power of the observed and calculated NOE intensities (James, 1991; Thomas et al., 1991; Brünger, 1993).

RESULTS

Exchangeable Proton Spectra. Exchangeable proton (amino, imino) resonance assignments were made in 90% H_2O/10% D_2O at 10 °C using a gradient-enhanced NOESY experiment that employs a double spin−echo sequence for water suppression with minimal saturation exchange (Hwang & Shaka, 1995; Callihan et al., 1996). Imino−imino and imino−H2 proton NOEs observed in these spectra (not shown) indicated normal base stacking in both the control and the ganciclovir-containing duplexes. Furthermore, interstrand imino proton and H2 proton to amino proton NOEs indicated normal Watson−Crick base pairing in both DNAs. These spectra also demonstrate that the imino proton of ganciclovir shows strong NOEs to the amino protons of the cytosine opposed to it in the duplex; thus, the base of ganciclovir appears to be normally hydrogen bonded with its complementary base.

Nonexchangeable Proton Spectra. The nonexchangeable base protons (purine H8 and pyrimidine H6) and the sugar protons (H1′, H2′, H2″, H3′, and H4′) for the control [d(CTGGATCCAG)]$_2$ and ganciclovir-containing [d(CTG-(ganciclovir)ATCCAG)]$_2$ decamers were assigned on the basis of an analysis of through-space distance connectivities in NOESY data sets as a function of mixing time and through-bond connectivities in COSY and TOCSY data sets recorded in D_2O buffer at 10 °C. The expanded NOESY (160 ms mixing time) contour plot establishing sequential connectivities between the base protons and the sugar H1′ protons of the ganciclovir-containing duplex is plotted in Figure 3A. The sequential connectivity patterns for the control decamer were very similar to those given in Nilges et al. (1987) (data not shown). The NOE connectivities from the base (purine H8 and pyrimidine H6) protons to its own (n) and 5′-flanking (n − 1) sugar H1′ protons have been traced along the ganciclovir-containing duplex starting at the 5′ end tracing through to the 3′ end (Figure 3A). (Note that since the duplex is self-complementary, there is only one set of resonances for the decamer strand; furthermore, the ganciclovir residue has two H1′ protons.) A similar sequential tracing could be made from the base protons to the H2′/H2″ protons (not shown).

The ^{1}H resonance assignments for the control and ganciclovir-containing decamers are given in Table 1. Corresponding assignments for the control decamer were not significantly different from those previously published (Nilges et al., 1987). Numerous significant (>0.1 ppm) chemical shift changes in the ganciclovir duplex compared to the control duplex were observed. Examination of the chemical shifts in Table 1 reveals large upfield chemical shift changes at the H3′/H3″ and H1′/H1″ protons of ganciclovir compared to the control duplex chemical shifts. This is not unexpected since protons on methine carbons are normally shifted downfield compared to the identical proton on a methylene carbon. Among the largest deviations in chemical shift were the H8 protons of ganciclovir(4) and A(5) which, compared to the control, were shifted 0.45 and 0.21 ppm upfield, respectively (Table 1). Other changes seen in Table 1 include the upfield shifts of 0.15, 0.19, and 0.13 ppm at the A(5)−H2″, A(5)−H3′, and the A(5)−H4′ protons, respectively. Significant downfield shifts included a 0.21 ppm shift at the imino proton of G(3), a 0.23 ppm shift at the T(6)−H6 proton, and 0.13 ppm at the G(3)−H2″ proton.

Phosphorus Spectra. A proton-decoupled phosphorus spectrum (not shown) of the ganciclovir-containing duplex revealed that most of the resonances were dispersed over a range from about −4.0 to about −4.6 ppm, which is characteristic of an unperturbed B-DNA phosphodiester backbone. One exception was a phosphorus resonance shifted downfield at about −2.6 ppm. The phosphorus resonances for the ganciclovir and control decamers were assigned from an analysis of 2-D heteroTOCSY experiments as previously described (Kellogg & Schweitzer, 1993). The heteroTOCSY spectrum obtained with the ganciclovir-containing duplex is included in Supporting Information. From this analysis, the phosphorus resonance at −2.6 ppm was assigned to the phosphate group immediately 3′ to the ganciclovir residue [i.e., at the ganciclovir(4)−A(5) step]. The remainder of the phosphorus assignments are listed in Table 2. Obviously, the greatest change in the phosphorus chemical shift is a 2.7 ppm downfield shift at the phosphorus between ganciclovir(4) and A(5). Other significant shifts (>0.2 ppm) were observed at two other residues and were both downfield shifts. These included a 0.26 ppm shift at the phosphorus between T(2) and G(3) and a 0.27 ppm shift at the phosphorus between C(8) and A(9).

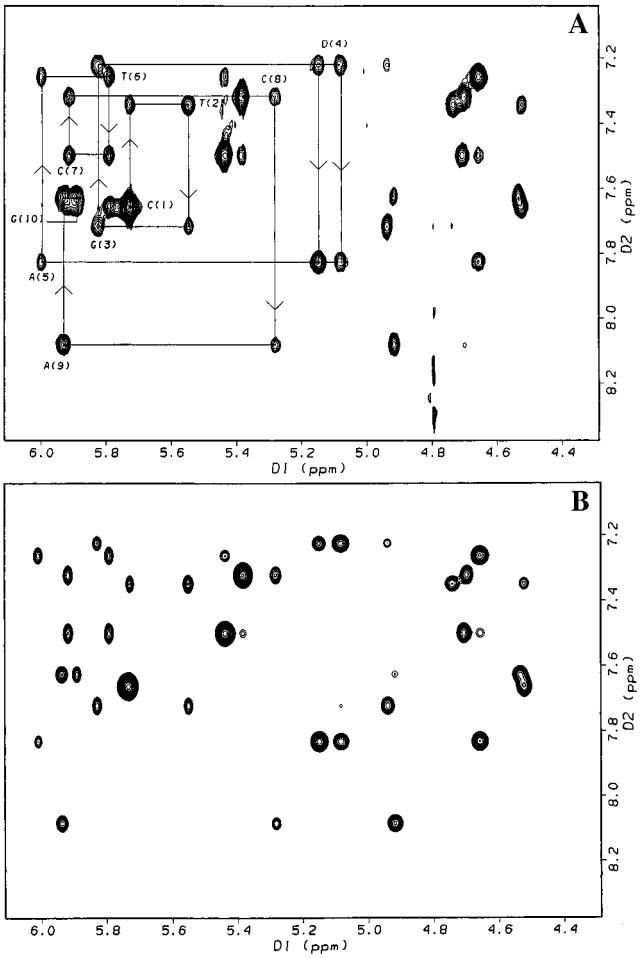

FIGURE 3: (A) Expanded NOESY (160 ms mixing time) contour plot of the ganciclovir duplex in D_2O at 10 °C. Shown are the connectivities between base protons and sugar H1′ protons. (B) Back-calculated NOESY (160 ms mixing time) contour plot of the H1′−H8/H6 region of the ganciclovir duplex. The back-calculated spectrum was generated from the relaxation matrix refined ganciclovir duplex structure possessing the lowest $R^{1/6}$ factor.

Sugar Puckers. A comparison of the control and ganciclovir NMR data suggests an atypical sugar conformation at the A(5) residue of the ganciclovir duplex. The strongest evidence for this perturbation came from the DQF-COSY data. In normal B-type DNA with C2′-endo sugar puckers,

Table 1: Proton Chemical Shifts in Control and Ganciclovir Decamers[a]

residue	H6/H8	H5/CH_3	H1′	H2′	H2″	H3′	H4′	imino	amino	H2
C1	7.70, 7.67	5.80, 5.86	5.78, 5.74	1.97, 1.98	2.42, 2.41	4.55, 4.53	3.97, 3.94		6.96, 7.80 (7.03, 7.80)	
T2	7.33, 7.34	1.55, 1.52	5.50, 5.55	1.96, 1.94	2.25, 2.30	4.72, 4.74	4.00, 4.03	13.98, 14.03		
G3	7.73, 7.72		5.45, 5.83	2.57, 2.58	2.63, 2.76	4.90, 4.94	4.22, 4.28	12.62, 12.84		
G4, D4	7.67, 7.22		5.56, 5.08/5.15	2.54, na	2.66, na	4.90, 4.03/4.08	4.29, 4.10	12.48, 12.50		
A5	8.04, 7.83		6.10, 6.00	2.48, 2.55	2.82, 2.67	4.85, 4.66	4.34, 4.21			7.64, 7.63
T6	7.03, 7.26	1.18, 1.07	5.79. 5.80	1.93, 2.04	2.37, 2.42	4.72, 4.66	4.02, 4.10	13.61, 13.47		
C7	7.38, 7.50	5.41, 5.44	5.83, 5.92	2.09, 2.04	2.29, 2.36	4.69, 4.71	4.06, 4.07		6.67, 8.34 (6.53, 8.19)	
C8	7.38, 7.32	5.52, 5.38	5.10, 5.28	1.90, 1.87	2.13, 2.17	4.68, 4.70	3.94, 3.98		6.75, 8.41 (6.61, 8.24)	
A9	8.08, 8.09		5.92, 5.94	2.62, 2.63	2.76, 2.79	4.91, 4.92	4.28, 4.28			7.66, 7.70
G10	7.63, 7.62		5.89, 5.90	2.13, 2.15	2.35, 2.36	4.52, 4.54	4.05, 4.07	na		

[a] Assignments are shown as control, ganciclovir. D4, DHPG. na, not applicable.

H3′−H4′ and H2″−H3′ couplings are weak and therefore produce weak cross-peaks in DQF-COSY and E.COSY spectra (Kim et al., 1992). In the DQF-COSY spectrum of the ganciclovir duplex, the A(5) residue exhibits strong H2″−H3′ and H3′−H4′ cross-peaks (Supporting Information) characteristic of an A-type C3′-endo sugar, whereas all other residues in this duplex and all residues in the control duplex had cross-peaks that were characteristic of the C2′-endo family (with the exception of the terminal residues which appear to have sugar puckers with A-type characteristics). These observations, along with differences noted between the A(5) cross-peaks in the control and ganciclovir NOESY spectra [e.g., a strong A(5) H2″−H4′ cross-peak in the ganciclovir spectrum (not shown)], lead us to conclude that the deoxyribose ring of the A(5) residue in the ganciclovir duplex has a conformation in the C3′-endo family. All other sugar conformations in the control and ganciclovir duplexes appear to be in the C2′-endo family, with the exception of the terminal residues which appear to have sugar puckers in between that of A- and B-type DNA.

Since the debate continues as to whether deoxyribose sugars exist in relatively fixed conformations, interconverting N and S puckers, or as an ensemble of conformations, we took the conservative approach of using the qualitative data described above to restrain sugars with relatively wide bounds in molecular dynamics calculations. Sugar puckers were approximated by a qualitative estimation of $J_{H2''-H3'}$ and $J_{H3'-H4'}$ from high-resolution DQF-COSY data and from NOESY-determined distances involving sugar protons (Wüthrich, 1986; Hosur et al., 1986; Kim et al., 1992; Schweitzer et al., 1994). Thus, the C(1), A(5), and G(10) sugars of the ganciclovir duplex were restrained to a pseudorotation angle range of 0−120° during dynamics calculations. All other sugars were restrained to a pseudorotation angle range as follows. Purines were given a pseudorotation angle range of 120−162° and pyrimidines a range of 100−162°. These values for the pseudorotation angle ranges were converted into ranges for the individual sugar torsion angles, ν, using the relationship $\nu_j = T_m \cos[P + 144(j - 2)]$, where j is 0−4 (Altona & Sundaralingam, 1980). These torsion angles were included in the restrained molecular dynamics calculations described below.

Restrained Molecular Dynamics. To understand the structural effects of ganciclovir in DNA at a quantitative level, restrained molecular dynamics simulations followed by full relaxation matrix refinement were performed. These calculations included the use of experimentally derived interproton distance and dihedral constraints and other restraints which preserve the right-handed nature of the helix and the base pairing within it. For both the control and the ganciclovir decamer, three calculations were performed starting from two different starting structures, one in a canonical A-type conformation (designated Ini-A) and one in a canonical B-type conformation (designated Ini-B). Different random number seeds were used for each calculation. The two starting structures for the simulations, Ini-A and Ini-B, have an atomic RMS deviation of 5.70 Å relative to each other.

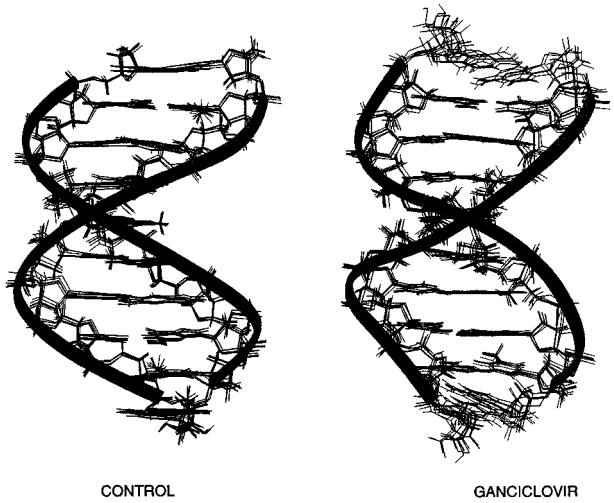

FIGURE 4: Overlay of the six final RR structures of the control duplexes (left) and the six final RR ganciclovir duplexes (right). Superimposed on the structures is a backbone ribbon trace based on the average of the six structures which highlights trends in backbone shape.

Full Relaxation Matrix Refinement. In the final stage of the structural refinement protocol, spin diffusion was taken into account by refining back-calculated, full relaxation matrix-derived NOESY intensities directly against the experimental data for each set of six control and ganciclovir rMD structures. For this refinement, a repel energy function was used for dynamical simulated annealing, followed by energy minimization using Lennard-Jones potentials, yielding the final structures shown in Figure 4. To ensure the accuracy of the final relaxation matrix refined (RR) structures, a NOESY spectrum was back-calculated from the relaxation matrix refined ganciclovir structure possessing the lowest $R^{1/6}$ factor among the six. Back-calculated spectra were simulated with the MODEL module of FELIX 95.0 (Molecular Simulations, Inc.) using the matrix doubling method. Shown in Figure 3 are the experimental and back-calculated fingerprint regions of the ganciclovir-containing duplex in the 160 ms NOESY experiment. Examination of the two spectra demonstrates excellent agreement in peak intensity between both. Other regions of the NOESY spectra exhibit similar levels of conformity (not shown). In the case

of the control decamer, the final six RR structures had an atomic RMS difference of 0.58 ± 0.18 Å. In the case of the ganciclovir-containing decamer, the final six RR structures had an atomic RMS difference of 0.73 ± 0.17 Å. The low RMSD between the structures in each set indicates that convergence to essentially a single structure had been obtained. Furthermore, the low RMSD between the structures derived from canonical A- or B-type DNA suggests that sufficient conformational space has been sampled during the molecular dynamics runs. Finally, $R^{1/6}$ factors were determined for the calculated structures. The $R^{1/6}$ factor of the calculated control structures was 0.047 ± 0.002 in comparison to 0.11 for ini-A and 0.081 for ini-B. The calculated ganciclovir structures had $R^{1/6}$ factors of 0.053 ± 0.002 in comparison to 0.124 for ini-A and 0.092 for ini-B. The clear reduction in $R^{1/6}$ factors for the calculated structures in comparison to starting structures demonstrates convergence to structures which are in excellent agreement with the experimental data.

Structural Analysis. (1) General Observations. Inspection of the final structures RR_{con} and $RR_{ganciclovir}$ in Figure 4 clearly shows that both sets of calculations have converged to B-type structures. Indeed, the control structures are very similar (1.8 Å RMSD) to canonical B-type DNA. The ganciclovir structures also resemble B-type DNA (2.2 Å RMSD) but exhibit some obvious distortions, including a kink in the backbone. This deviation from the control structure extends from ganciclovir(4) to T(6) before returning to approximately the control conformation. The ganciclovir duplex also appears to be slightly underwound compared to the control structure, and the ends of the helix are slightly bent into the major groove.

(2) Helical Parameters. Analyses of the helical parameters of the relaxation matrix-refined structures were carried out with the Curves (Lavery & Sklenar, 1988, 1989) module of the structural analysis program Dials-and-Windows (Ravishanker et al., 1989). Values for selected intrabase and interbase pair helical parameters as a function of base pair number are shown in Figure 5. Values for helical parameters such as propeller twist and rise were nearly identical in the control and ganciclovir structures and therefore are not shown. Inspection of Figure 5 reveals that most of the deviations in helical parameters occur at ganciclovir(4) or at A(5), immediately 3′ to the lesion site. These perturbations will be discussed in more detail below.

(3) Base Stacking. The stacking of four base pair steps centered around the G(4) residue in the refined control structure and the refined ganciclovir structure with the lowest $R^{1/6}$ factors can be viewed in Figure 6. The stacking in the control structure is consistent with a B-type double helix in which purine−pyrimidine steps demonstrate a high degree of intrastrand overlap and little intrastrand base overlap at pyrimidine−purine base steps. Purine−purine steps exhibit a modest degree of intrastrand base overlap, while pyrimidine−pyrimidine steps show virtually no intrastrand base overlap. In $RR_{ganciclovir}$, the ganciclovir residue is positioned in the helix such that an increase in stacking occurs between the base of G(3) and the base of ganciclovir(4). A small increase in base stacking is also seen between the base of ganciclovir(4) and the base of A(5). Stacking in the remainder of the $RR_{ganciclovir}$ structure closely resembles that of the control structure RR_{con}.

(4) Backbone Torsion Angles. As described in Materials and Methods, the backbone torsion angles involving the ganciclovir residue were not restrained at any point of the calculations nor were the corresponding angles in the control structure; furthermore, no backbone restraints were used for any residues during the relaxation matrix refinement. Average values of the backbone torsion angles, α, β, γ, ϵ, δ, and ζ as well as the glycosidic torsion angle χ and the pseudorotation angle P for the RR_{con} and $RR_{ganciclovir}$ structures are given in Table 3, sections A and B, respectively. Examination of backbone torsion angles reveals significant changes in the ganciclovir duplex with respect to the control duplex. The majority of these deviations occurred at the lesion site or at residues G(3) and A(5) located immediately 5′ or 3′ to the lesion site, respectively. It is interesting to note that the backbone torsion angles for the residues base-paired with G(3), ganciclovir(4), and A(5) [i.e., T(6)−C(8)] showed minor, if any, deviation from control values. The remainder of the duplex also possessed torsion angles consistent with that of the control structure.

(5) Glycosidic Torsion Angles. The glycosidic torsion angle χ was not restrained at any point in the dynamics calculations. In the control structure RR_{con} structures, χ angles were all in the range of 240°, which is characteristic of B-type DNA (Table 3). The $RR_{ganciclovir}$ structures also exhibited B-type χ angles with the exception of ganciclovir (4) and its 3′ A(5) residue. The largest deviation in the glycosidic torsion occurred at the lesion site. This torsion angle of 126° did not resemble A-DNA (χ = 206°) or B-DNA (χ = 262°). The A(5) χ angle was also distorted with a value of 214°, which is characteristic of A-type DNA. Glycosidic torsion angles returned to normal B-type DNA at the T(6) residue.

(6) Sugar Pucker. All the sugar residues in the control duplex with the exception of the terminal residues have sugar pucker values in the range of 140−160° corresponding with C2′-endo conformations (Table 3). Pseudorotation angles for the sugar residues of the ganciclovir duplex were all observed to range between 140° and 160° with the exception of the terminal residues C(1) and G(10) and the A(5) residue 3′ to the ganciclovir lesion. Pseudorotation angles between 80° and 90° for the terminal residues are consistent with that of the control duplex; furthermore, this type of pucker at terminal residues is commonly observed in DNA solution structures. However, the pseudorotation angle observed at the A(5) residue was 51°, indicating a C3′-endo sugar conformation.

DISCUSSION

NOE and Chemical Shift Patterns in the Ganciclovir-Containing Duplex. Qualitative NOE analysis revealed the general pattern of $NOE_{H2'(i)-H8/H6(i)} \gg NOE_{H2''(i-1)-H8/H6(i)} > NOE_{H2'(i-1)-H8/H6(i)}$ which is characteristic of right-handed B-type structures. Furthermore, examination of NOESY spectra acquired in H_2O demonstrates that all residues, including ganciclovir, exhibit normal Watson−Crick base pairing. Although thermal melting experiments have shown that the ganciclovir-containing duplex has reduced stability (Marshalko et al., 1995), the NOESY data show that the base of ganciclovir is normally hydrogen bonded with its complementary base, so the instability is probably due to factors other than a disruption of this base pair. Thus, the NMR data indicate that the introduction of a ganciclovir residue

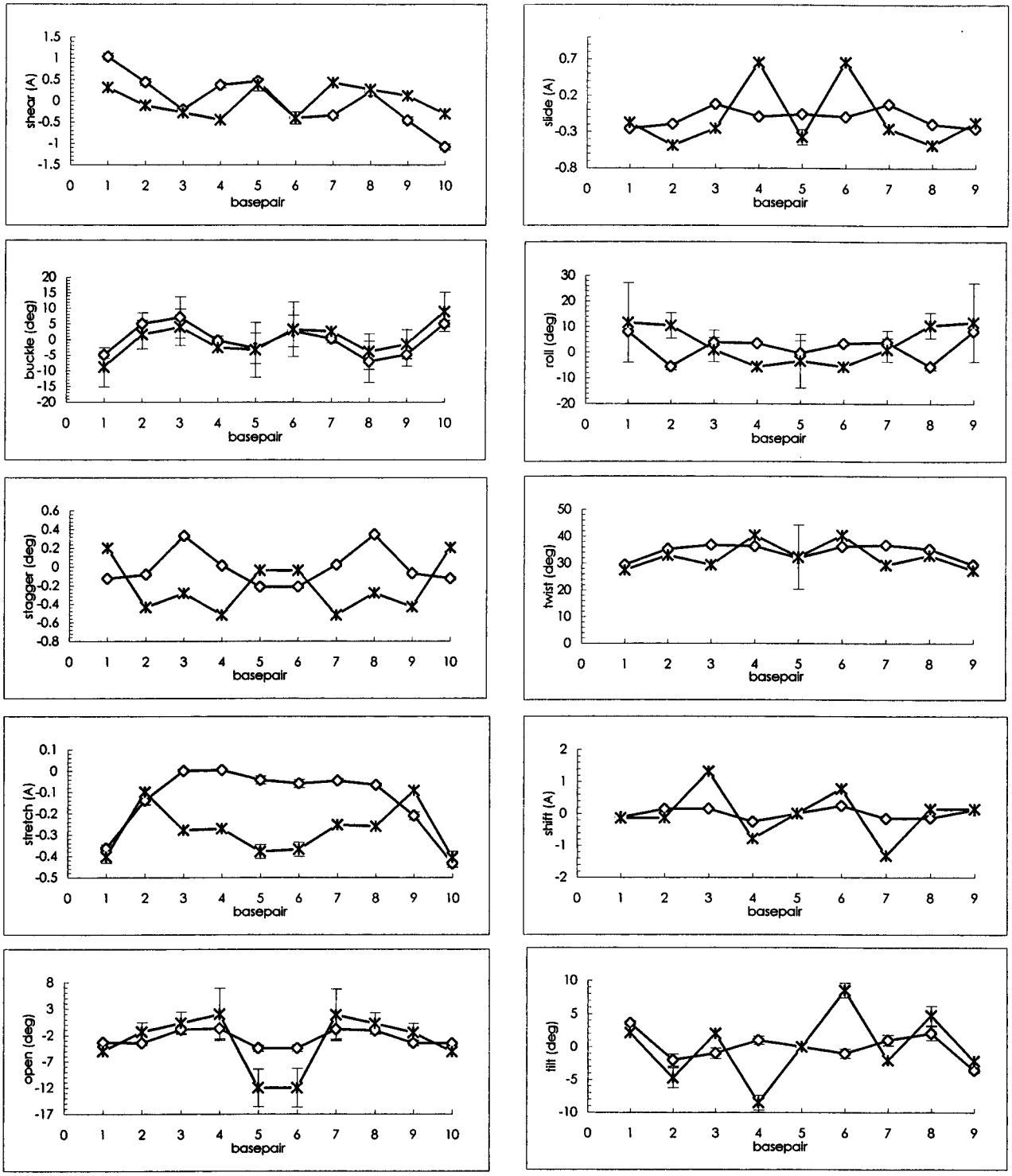

FIGURE 5: Comparison of the helical parameters of the $RR_{control}$ and $RR_{ganciclovir}$ structures. The helical parameter values for the six control and ganciclovir structures were averaged and plotted as shown. The variance ($[(\sum x_i + x_{i+1})^2/(n-1)]$) between the six final RR structures is shown within brackets. Parameter values were calculated using CURVES (Lavery & Sklenar, 1988, 1989). Symbols: (◇) RR_{con}; (*) $RR_{ganciclovir}$.

into DNA does not distort the global conformation of the helix. It is therefore not surprising that the calculated structure of the ganciclovir-containing duplex, while exhibiting a number of local distortions, is obviously B-type in overall conformation. These qualitative observations support our previous results using CD spectroscopy and chemical probes (Marshalko et al., 1995). Additional qualitative observations made from the NOESY spectra are also supported in the refined $RR_{ganciclovir}$ structures. For example, an H1′ proton on ganciclovir(4) shows a strong interresidue cross-peak with the H8 proton of A(5) (Figure 3A). In $RR_{ganciclovir}$, these two protons are only 2.6 Å apart (Figure 7), which is nearly 1 Å shorter than the corresponding protons in the control structure. In addition, the H2″ proton of A(5) has a much weaker intraresidue NOE cross-peak with the H8 proton than is seen in the control spectrum (not shown). In $RR_{ganciclovir}$, these protons are almost 4.5 Å from each other, which is unusually far apart for B-type duplexes and 1 Å farther than seen in the control structure. Arguably the best evidence that our calculated structures are accurate representations of the actual time-averaged solution structure is that the back-calculated spectra are

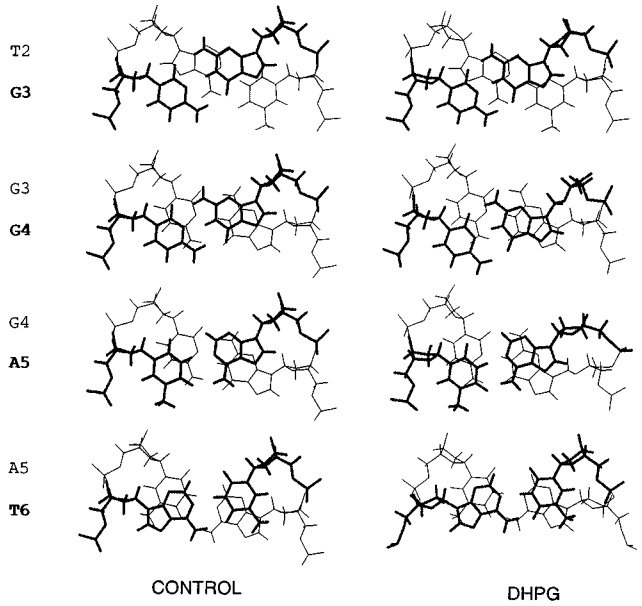

FIGURE 6: Base stacking in the lowest $R^{1/6}$ factor control RR structure (left) and the ganciclovir RR structure (right). Base pairs 2−6 are shown viewed down the global helical axis. The first base pair in the stack is shown with bold lines.

Table 2: Phosphorus Chemical Shifts[a] in Control and Ganciclovir Decamers

position	dinucleoside	control (ppm)	ganciclovir (ppm)
1	CpT	−4.38	−4.36
2	TpG	−4.06	−4.08
3	GpG	−4.04	−4.15
4	GpA	−4.20	−2.62
5	ApT	−4.54	−4.55
6	TpC	−4.40	−4.46
7	CpC	−4.27	−4.37
8	CpA	−3.86	−3.98
9	ApG	−4.24	−4.19

[a] Phosphorus chemical shifts are referenced to external 10% trimethyl phosphate at 10 °C.

nearly identical to the experimental NOESY spectra (Figure 3).

The refined structure of the ganciclovir-containing duplex also has features that are consistent with the changes in chemical shift from control values shown in Table 1. For example, a large (0.45 ppm) upfield chemical shift is seen for the H8 proton of ganciclovir(4). In our model, the H8 proton of ganciclovir is positioned over the perimeter of the G(3) aromatic ring in comparison to the control G(4) H8 which is clearly offset from the G(3) aromatic ring system (Figure 6). This increase in stacking at the lesion site is consistent with the observed upfield chemical shift. A small increase in base stacking is also seen between the base of ganciclovir(4) and the base of A(5), consistent with the upfield chemical shift of the H8 proton of A(5). In addition, the O4′ oxygen of ganciclovir makes a close approach to this H8 proton, which might also contribute to the observed change in chemical shift. Similarly, chemical shifts of the sugar protons of A(5) and the aromatic protons of T(6) correlate well with close contacts (<2 Å) or other structural changes that are observed in the ganciclovir structure but not in the control duplex.

The greatest change in the phosphorus chemical shift is a 2.7 ppm downfield shift at the phosphorus between ganciclovir(4) and A(5). We have recently shown using ^{31}P relaxation measurements that there is an apparent correlation between ^{31}P chemical shift, ^{31}P T_2 values, and backbone mobility (Schweitzer et al., 1995). This correlation predicts that increased mobility or disorder at a particular site in the backbone results in a downfield ^{31}P chemical shift at that site. The large downfield shift that we actually observe at the phosphorus between ganciclovir(4) and A(5) is therefore consistent with significantly increased disorder in the backbone at this position**,** which was not unexpected considering the additional freedom of movement permitted by the acyclic lesion. Measurements of the ^{31}P T_1, T_2, and $T_{1\rho}$ are in progress to examine this issue in more detail.

Structural Features. (1) Control Duplex. The structural features of RR_{con} are quite similar to those reported by Nilges et al. (1987) for the same sequence. This is not surprising since very similar methods were used to collect and analyze the data. The only significant differences between the studies is that our data were collected at 10 °C rather than 25 °C and that our structures were refined by relaxation matrix calculations. Despite these differences, very similar trends in helical parameters such as roll, helical twist, tilt, and slide were observed in both studies. Base stacking patterns were nearly identical, and most torsion angles were in close range of one another. One difference that we noted is pseudorotation angles of 100° for the T6 and A9 residues in the structure reported by Nilges et al. (1987), while these pseudorotation angles are between 145° and 150° in our structure, closer to canonical B-type values. It is possible that the higher temperature used in the earlier study may have contributed to this discrepancy.

(2) Ganciclovir-Containing Duplex. The most striking change in the structure of the ganciclovir-modified duplex is an obvious kink in the backbone that extends from ganciclovir(4) to T(6) (Figure 4). As shown in Figure 5, this kink is associated with a number of perturbations in helical parameters such as base pair shear, slide, tilt, shift, and open, which exhibit maximum deviations from control values in this region. In the case of ganciclovir, the base attached to the acyclic sugar has additional degrees of freedom; consequently, steric clashes in the ganciclovir-containing duplex can be relieved in ways that are not available in the control duplex. Some of the above parameters also reflect the increased stacking that is observed in this region of the duplex. Again, the additional conformational flexibility at the acyclic lesion site may be permitting these additional interactions.

The region associated with the kink in the backbone has a number of features that more closely resemble A-type DNA than B-type. For example, inspection of Figure 5 reveals an A-type stretch at the A(5)/T(16) and the T(6)/A(15) base pairs. Furthermore, the helix is significantly underwound at the lesion site; twist at ganciclovir(4) reaches a helical minimum of 28° in comparison to 36° for standard B-type DNA. Particularly striking in its similarity to an A-type residue is the conformation of residue A(5). Backbone torsion angles α, β, δ, and ζ clearly show an A-type conformation in the backbone of this residue. The sugar pucker of the A(5) residue in the refined ganciclovir structure is also in the C3′-endo or A-type family (P = 51°). In addition, the glycosidic torsion angle χ of A(5) is 214°, which is closer to A-DNA (χ = 206°) than to B-DNA (χ = 262°), while the corresponding χ angle in the control duplex is 246°. Of course, there are also many unusual torsion angles observed at the lesion site itself. In this case, however, it needs to be emphasized that the structures presented here

Table 3: Backbone Torsion Angles,[a] Glycosidic Torsion Angle χ, and Pseudorotation Angle P of Averaged Relaxation Matrix Refined Structures

residue	α	β	γ	δ	ϵ	ζ	χ	P
				(A) Control Structure RR_{con}				
C1	294[6.0]	180[7.1]	61[1.2]	100[1.2]	180[6.8]	275[5.1]	221[3.3]	88[1.4]
T2	291[3.9]	192[3.5]	61[0.65]	131[0.99]	170[0.92]	263[1.8]	245[1.7]	147[0.92]
G3	292[6.8]	190[3.5]	51[1.0]	130[2.7]	169[2.7]	272[2.4]	249[4.0]	148[2.8]
G4	286[2.4]	192[4.0]	59[1.7]	130[0.58]	168[3.7]	266[1.5]	247[0.67]	149[0.86]
A5	290[4.8]	175[3.3]	63[3.2]	135[0.89]	179[3.6]	255[3.6]	246[2.0]	152[1.3]
T6	284[4.8]	191[3.2]	60[1.5]	130[0.83]	171[2.1]	268[2.7]	240[2.5]	144[0.60]
C7	290[1.1]	188[2.5]	59[0.85]	130[2.0]	173[2.0]	267[2.1]	242[0.93]	147[2.6]
C8	285[6.0]	206[5.0]	58[2.6]	131[0.33]	157[3.7]	272[2.7]	243[1.4]	148[0.37]
A9	271[7.1]	189[3.0]	56[4.0]	132[0.60]	171[4.5]	272[1.6]	251[0.54]	151[0.27]
G10				100[1.4]			231[4.0]	89[1.8]
mean	287	189	59	125	171	268	242	136
SD[b]	6.9	8.6	3.5	13	6.7	6.0	9.0	25
A-DNA[c]	285	208	45	83	178	313	206	13
B-DNA[d]	314	214	36	156	155	264	262	191
				(B) Ganciclovir Structure $RR_{ganciclovir}$				
C1	286[2.5]	177[4.0]	67[2.2]	98[0.97]	173[4.4]	280[2.3]	233[1.8]	85[1.6]
T2	267[4.4]	195[2.9]	61[2.0]	133[0.71]	177[1.8]	267[2.5]	247[0.83]	146[0.69]
G3	215[85]	197[38]	87[36]	130[0.72]	178[7.7]	271[21]	250[2.8]	144[0.82]
G4	269[16]	157[23]	17[11]	NA	260[68]	260[151]	126[9.4]	NA
A5	287[2.4]	192[3.9]	68[2.0]	86[2.1]	162[3.9]	294[2.0]	214[3.1]	51[2.9]
T6	283[2.0]	177[2.2]	67[2.9]	136[0.54]	180[0.83]	269[0.82]	236[1.1]	155[0.79]
C7	288[2.6]	183[4.7]	61[2.0]	133[1.9]	181[3.2]	247[4.5]	252[5.1]	151[2.3]
C8	271[6.6]	207[5.4]	51[1.4]	137[0.77]	170[2.6]	276[2.5]	247[1.5]	155[1.4]
A9	280[4.0]	170[6.3]	52[3.0]	131[0.55]	191[11]	261[2.1]	263[2.3]	149[0.18]
G10				100[0.96]			239[6.5]	88[6.5]
mean	272	184	59	120	186	269	231	125
SD[b]	23	15	19	20	29	13	39	39
A-DNA[c]	285	208	45	83	178	313	206	13
B-DNA[d]	314	214	36	156	155	264	262	191

[a] Backbone torsion angles are defined as P(i)−α−O5′−β−C5′−γ−C4′−δ−C3′−ϵ−O3′−ζ−P(i + 1). [b] SD, standard deviation. [c] Canonical A-DNA (Arnott & Hukins, 1972). [d] Canonical B-DNA (Arnot & Hukins, 1973). Values are shown as average[SD].

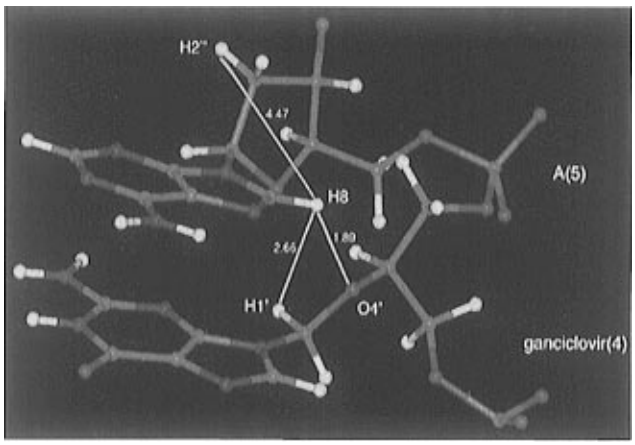

FIGURE 7: Expanded view of the ganciclovir residue and adjacent A(5) residue in the ganciclovir RR structure with the lowest $R^{1/6}$ factor. Atom colors are represented as follows: red, oxygen; green, carbon; blue, nitrogen; white, hydrogen; pink, phosphorus. Selected distances shown are in angstroms.

represent time-averaged conformations. This is especially important to keep in mind when considering the structure of the backbone near the lesion site where the conformation is primarily driven by the empirical force field and a few experimental restraints. Undoubtedly, there are other conformations that may be possible at this site, but longer simulations in the presence of solvent and counterions will probably be necessary before this issue can be clarified.

This finding of a residue with an A-type conformation 3′ to an acyclic lesion is reminiscent of the results of structural studies on a DNA duplex containing an abasic site. In this structure, the sugar conformation of the residue 3′ to the lesion site is shifted toward the C3′-endo conformation and the phosphate backbone is distorted toward an A-type conformation (Cuniasse et al., 1989). *Thus, two types of lesions that introduce additional degrees of freedom into the helix result in a distortion of the residue 3′ to the lesion site to an A-type conformation.* In this earlier study, it was postulated that rather than adopting a uniquely C3′-endo conformation, the conformational equilibrium of the sugar 3′ to the abasic site had been displaced to a point where there was a greater than normal fractional contribution of the C3′-endo state. A similar situation has been hypothesized for terminal residues in DNA duplexes; these residues have less structural restraints than residues in the core of the duplex, and they exhibit sugar puckers in between that of C2′-endo and C3′-endo conformation. Furthermore, ^{13}C relaxation measurements have indicated that sugars of terminal residues are more disordered than sugars in the core (Borer et al., 1994); thus, their intermediate sugar pucker may be a time average of a continuum of rapidly fluctuating conformers. We will be carrying out ^{13}C and ^{31}P relaxation studies on the ganciclovir-containing duplex in order to determine whether the distortions that we observe in the structure are static or dynamic in nature.

Biochemical Implications of the Ganciclovir Solution Structure. Biochemical investigations employing a variety of DNA polymerases, including HSV-1 DNA polymerase (Frank et al., 1984), HSV-2 DNA polymerase (Reid et al., 1988), CMV DNA polymerase (Reid et al., 1988), and the Klenow fragment of *E. coli* DNA polymerase I (Marshalko et al., unpublished results) as well as mammalian DNA polymerase α (Reardon, 1989; Isley et al., 1995), polymerase δ, and polymerase ϵ (Isley et al., 1995), have shown that the triphosphate of ganciclovir can compete effectively with dGTP for incorporation into DNA. Unlike the action of

araCTP, the incorporation of ganciclovir by these polymerases does not result in absolute chain termination but instead results in N + 1 arrest, where one additional dNTP is added to ganciclovir followed by inhibition of further polymerization. The solution structure of the ganciclovir-containing DNA duplex that we have determined provides some possible explanations for this unusual type of polymerization inhibition. In this structure, the base of ganciclovir appears to be normally hydrogen bonded and stacked in the double helix; however, the NMR data and the structure calculated from these data clearly show that the residue 3′ to the lesion site is in an unusual A-type conformation. The presence of this A-type residue in a B-type duplex contributes to the distinct kink in the backbone at this site. Extrapolating from an NMR structure of a self-complementary duplex structure containing two analog residues to explain what might be occurring at a primer-template junction complexed with a polymerase needs to be done with caution. Nevertheless, it is reasonable to hypothesize that most DNA polymerases would pause at a site exhibiting the type of distortion described above rather than continue polymerization.

SUPPORTING INFORMATION AVAILABLE

Five figures showing an expanded DQF-COSY contour plot of the H3′−H4′ region of the control duplex, an expanded DQF-COSY contour plot of the H3′−H4′ region of the ganciclovir duplex, an expanded DQF-COSY contour plot of the H2′/H2″−H3′ region of the control duplex, an expanded DQF-COSY contour plot of the H2′/H2″−H3′ region of the ganciclovir duplex, and a heteroTOCSY contour plot of the ganciclovir duplex at 10 °C (6 pages). Ordering information is given on any current masthead page.

REFERENCES

Altona, C., & Sundaralingam, M. (1972) *J. Am. Chem. Soc. 94*, 8205−8212.

Arnott, S., & Hukins, D. W. (1972) *Biophys. Biochem. Res. Commun. 47*, 1504−1509.

Arnott, S., & Hukins, D. W. (1973) *J. Mol. Biol. 81*, 93−105.

Baleja, J. D., Pon, R. T., & Sykes, B. D. (1990) *Biochemistry 29*, 4828−39.

Borer, P. N., LaPlante, S. R., Kumar, A., Zanatta, N., Martin, A., Hakkinen, A., & Levy, G. C. (1994) *Biochemistry 33*, 2441−2450.

Brooks, B. R., Bruccoleri, R. E., Olafson, B. D., States, D. J., Swaminathan, S., & Karplus, M. (1983) *J. Comput. Chem. 74*, 187−217.

Brunger, A. T. (1993) *X-PLOR 3.1: A System for Crystallography and NMR*, Yale University, New Haven, CT.

Buckner, F. S., & Pomeroy, C. (1993) *Clin. Infect. Dis. 17*, 644−656.

Callihan, D., West, J., Schweitzer, B. I., & Logan, T. M. (1996) *J. Magn. Reson., Ser. B 112*, 82−86.

Chen, S. H., Shine, H. D., Goodman, J. C., Grossman, R. G., & Woo, S. L. (1994) *Proc. Natl. Acad. Sci. U.S.A. 91*, 3054−3057.

Clore, G. M., Hartmut, O., McLaughlin, L. W., Benseler, F., Happ, C. S., Happ, E., & Gronenborn, A. M. (1988) *Biochemistry 27*, 4185−4197.

Culver, K. W., Ram, Z., Walbridge, S., Ishii, H., Oldfield, E. H., & Blaise, R. M. (1992) *Science 256*, 1550−1552.

Culver, K. W., Van Gilder, J., Link, C. J., Carlstrom, T., Buroker, T., Yuh, W., Koch, K., Schabold, K., Doornbas, S., Wetjen, B., & Blaise, R. M. (1994) *Hum. Gene Ther. 5*, 343−379.

Cuniasse, Ph., Sowers, L. C., Eritja, R., Kaplan, B., Goodman, M. F., Cognet, J. A. H., Le Bret, M., Guschlbauer, W., & Fazakerley, G. V. (1989) *Biochemistry 28*, 2018−2026.

DiMaio, J. M., Clary, B. M., Bia, D. F., Coveney, E., Pappas, T. N., & Lyerly, H. K. (1994) *Surgery 116*, 205−213.

Emmanuel, D. (1990) *Semin. Hematol. 27*, 22−27.

Erice, A., Jordan, M. C., Chace, B. A., Fletcher, C., Chinnock, B. J., & Balfour, H. H. (1987) *JAMA, J. Am. Med. Soc. 257*, 3082−3087.

Faulds, D., & Heel, R. C. (1990) *Drugs 39*, 597−638.

Frank, K. B., Chiou, J. F., & Cheng, Y. C. (1984) *J. Biol. Chem. 259*, 1566−1569.

Gronenborn, A. M., & Clore, G. M. (1989) *Biochemistry 28*, 5978−5984.

Hasegawa, Y., Emi, N., & Shimokata, K. (1995) *J. Mol. Med. 73*, 107−112.

Holak, T. A., Engstrom, A., Draulis, P. J., Lindeberg, G., Bennich, H., Jones, A., Gronenborn, A. M., & Clore, G. M. (1988) *Biochemistry 27*, 760−769.

Hwang, T. L., & Shaka, A. J. (1995) *J. Magn. Reson. 112A*, 275−279.

Ido, A., Nakata, K., Katau, Y., Nakao, K., Murata, K., Fujita, M., Ishii, N., Tamaoki, T., Shiku, H., & Nagataki, S. (1995) *Cancer Res. 35*, 3100−3109.

Isley, D. D., Lee, S. H., Miller, W. H., & Kucha, R. D. (1995) *Biochemistry 34*, 2504−2510.

James, T. L. (1991) *Curr. Opin. Struct. Biol. 1*, 1042−53.

Karkas, J. D., Germaershausen, J., Tolman, R. L., MacCoss, M., Wagner, A. F., Liou, R., & Bostedor, R. (1987) *Biochim. Biophys. Acta 911*, 127−135.

Kellogg, G. W., & Schweitzer, B. I. (1993) *J. Biomol. NMR 3*, 577−595.

Kim, S.-G., Lin, L.-J., & Reid, B. R. (1992) *Biochemistry 31*, 3564−3574.

Lavery, R., & Sklènar, H. (1988) *J. Biomol. Struct. Dyn. 6*, 63−91.

Lavery, R., & Sklènar, H. (1989) *J. Biomol. Struct. Dyn. 6*, 655−667.

Manome, Y., Abe, M., Hagen, M. F., Fine, H. A., & Kufe, D. W. (1994) *Cancer Res. 54*, 5408−5413.

Marshalko, S. J., Schweitzer, B. I., & Beardsley, G. P. (1995) *Biochemistry 34*, 9235−9248.

Nevins, T. E., & Dunn, D. L. (1992) *J. Am. Soc. Nephrol. 2*, S270-S273.

Nilges, M., Clore, G. M., Gronenborn, A. M., Brünger, A. T., Karplus, M., & Nilsson, L. (1987a) *Biochemistry 26*, 3718−3733.

Nilges, M., Clore, G. M., Gronenborn, A. M., Piel, N., & McLaughlin, L. W. (1987b) *Biochemistry 26*, 3734−3744.

Nilges, M., Hazabettl, J., Brünger, A. T., & Holak, T. A. (1991) *J. Mol. Biol. 219*, 499−510.

Ravishanker, R., Swaminathan, S., Beveridge, R. L., & Sklenar, H. (1989) *J. Biomol. Struct. Dyn. 6*, 669−699.

Reardon, J. E. (1989) *J. Biol. Chem. 264*, 7405−7411.

Reid, R., Mar, E. C., Huang, E. S., & Topal, M. D. (1988) *J. Biol. Chem. 263*, 3898−3905.

Rosenberg, J. M., Seeman, N. C., Day, R. O., & Rich, A. (1976) *J. Mol. Biol. 104*, 145−167.

Schweitzer, B. I., Mikita, T., Kellogg, G. W., Gardner, K. H., & Beardsley, G. P. (1994) *Biochemistry 33*, 11460−11475.

Schweitzer, B. I., Gardner, K. H., & Tucker-Kellogg, G. (1995) *J. Biomol. NMR 6*, 180−188.

Seeman, N. C., Rosenberg, J. M., Suddath, F. L., Kim, J. J. P., & Rich, A. (1976) *J. Mol. Biol. 104*, 109−144.

Smythe, W. R., Hwang, H. C., Amin, K. M., Eck, S. L., Davidson, B. L., Wilson, J. M., Kaiser, L. R., & Albelda, S. M. (1994) *Cancer Res. 54*, 2055−2059.

States, D. J., Haberkorn, R. A., & Ruben, D. J. (1982) *J. Magn. Reson. 48*, 286−292.

Thomas, P. D., Basus, V. J., & James, T. L. (1991) *Proc. Natl. Acad. Sci. U.S.A. 88*, 1237−1241.

Tolman, R. L. (1989) in *Nucleotide Analogues As Antiviral Agents* (Martin, J. C., Ed.) pp 35−50, American Chemical Society, Washington, DC.

Wüthrich, K. (1986) in *NMR of Proteins and Nucleic Acids*, pp 203−255, John Wiley & Sons, New York.

Yip, P., & Case, D. A. (1989) *J. Magn. Reson. 83*, 643−648.

Yoshida, K., Kawami, H., Yamaguchi, Y., Kuniyasu, H., Nishiyama, M., Hirai, T., Yanagihara, K., Tahara, E., & Toge, T. (1995) *Cancer 75*, 1467−1471.

Zaia, J. S. (1993) *Clin. Infect. Dis. 17*, S392−399.

BI962604E